A Stress-Deformation based Algorithm for Quasi-Static Designing Unreinforced Unpaved Roads Incorporating Operational Stabilities

Nayan Jyoti Sarma

Research Scholar, Department of Civil Engineering, Indian Institute of Technology Guwahati, Guwahati, Assam, India. Email: nayan.jyoti@iitg.ac.in

Arindam Dey

Associate Professor, Department of Civil Engineering, Indian Institute of Technology Guwahati, Assam, India. Email: arindamdeyiitg16@gmail.com

ABSTRACT

This paper presents a coupled stress-deformation based algorithm in a finite element framework for quasi-static designing of unreinforced unpaved roads comprising generalized subgrade. In contrary to the traditional limit equilibrium based design that considers only the undrained shear strength of the soft cohesive subgrades, this algorithm considers both frictional (φ) and cohesive (c) components of subgrade shear strength. Further, in contrary to the conservative assumption of non-deformability of subgrade and aggregate layers in the earlier approach, this algorithm considers the deformability based operational failure of individual components of unpaved road section. In the algorithm, the limiting strength parameters of aggregate and subgrade are to be identified that would ensure the operational stability of the natural subgrade under aggregate loading as well as the stability of the aggregate layer under quasi-static vehicular loading. Even after the operational stabilities are ensured, weaker subgrades when subjected to heavier axle loads has the tendency to exhibit failure due to the transmission of the secondary stresses, which is also considered in the design algorithm. The coupled stress-deformation based design algorithm reported herein provides a comprehensive design approach duly incorporating all such operational failure conditions.

Keywords: Unreinforced unpaved roads; Coupled stress-deformation approach; Finite element analysis; Operational stability; Secondary stress; Design algorithm

Introduction

For many developed and developing countries around the world, significant stretches of unpaved (or, unsurfaced) roads are managed by the national authorities. As per the Central Intelligence Agency (CIA) world fact-book (2016), approximately 79% of the total road network in South Africa comprises unpaved roads, while the same is around 35% for USA (CIA, 2012) and approximately 45-50% in India (MORTH, 2023). There are various types of unpaved roads (including dirt roads, haul roads and access roads), out of which the most common is the one where a gravel layer, lateritic soil layer or even a layer of tire-reinforced recycled aggregates is placed directly over the natural soil subgrade (Paige-Green *et al*., 2015; Mendoza *et al*., 2022) without the application of any permanent surfacing such as those given for an asphalt or concrete pavement. Unpaved roads are supposed to carry lesser volume of traffic and, customarily, if the traffic exceeds about 300 vehicles per day, it is often economically viable to surface them with a bituminous seal (Richards, 1978). Although the quality of service from the unpaved roads is expectedly lower in comparison to paved roads, yet it provides a major transportation carriageway to support the movements of goods and carriage vehicles in the lesser accessible areas. Although an economically viable option for lower volume traffic, there are cases where unpaved roads have to sustain heavier vehicles such as the roads connecting a large industrial plant to a major road, approach roads to newly constructed sites and embankments, major village roads connecting to nearby highway, heavy vehicle roads inside forest areas etc. In most cases, unpaved roads have to laid on natural soil subgrades with insufficient bearing resistance against heavily loaded vehicles, and consequently undergoes short-term or long-term distresses leading to potholes, rutting, corrugation, washboard formations, surface degradation and dust emission (Alzubaidi and Magnusson, 2002; Shoop *et al*., 2006; Edvardsson, 2009; Jones 2015; le Vern 2022; Ibagon *et al*., 2023). In order to prolong the performance life of such roads (as indicated by Jones, 2015; Huber *et al*., 2020), it is important that an engineered design methodology of unpaved roads is developed by incorporating the geotechnical characteristics of the bearing subgrade. In this regard, although some studies are conducted over the years, a thorough geotechnics-based analysis is yet pending for the same.

Giroud and Noiray (1981) pioneered a design methodology for unpaved roads resting on a saturated cohesive subgrade with low permeability. The thickness of the aggregate layer was

63 estimated by adopting a quasi-static approach, which is based on the stress transferred through the
64 aggregate layer following a load dispersion mechanism and subsequently resisted by the undrained
65 shear strength of the subgrade. Furthermore, the increment in the required aggregate layer
66 thickness due to repeated passages of traffic was also estimated for a specified rut depth of 50 mm.
67 Holtz and Sivagukan (1987) extended the work by incorporating a wider practical range of rut
68 depths (75 mm – 300 mm) to estimate the aggregate layer thickness for unpaved roads subjected
69 to standard axle load and varying tire pressures. For both plane-strain and axisymmetric loading
70 conditions, Miligan *et al*. (1989a, 1989b) further extended the pioneering work of Giroud and
71 Noiray (1981) by considering the development of horizontal outward shear stresses at the
72 subgrade-fill interface due to the applied quasi-static vertical load. Boresi and Palmer (1995)
73 presented a review of the design methodologies for unpaved roads existing in that era, which
74 indicated that the WES models, based on rut-depth as the major failure criterion (incorporating
75 subgrade, aggregate and traffic parameters), were best suited in assessing the thickness of the
76 aggregate layer of unpaved roads (Barber *et al*., 1978; U.S. Army Corps of Engineer Waterways
77 Experiment Station, 1978). Based on the research on South African roads, Paige-Green (1990)
78 provided a guideline on the design of unpaved roads while primarily focusing on the construction
79 and maintenance. Douglas and Valsangkar (1992) proposed to use the stiffness of the unpaved
80 road as the key design criterion instead of the rut depth, as the latter can be eradicated by a periodic
81 maintenance of unpaved road. Based on the concept proposed by Milligan *et al*. (1989a) and its
82 subsequent calibration through the numerical analyses results of Burd and Frydman (1997), an
83 empirical relation of equivalent load spread angle was proposed for unreinforced unpaved roads
84 resting over soft subgrade and subjected to monotonic loading condition (Houlsby and Burd,
85 1999). The equivalent load dispersion angle was established as a function of friction angle of the
86 granular fill and the ratio of subgrade strength to the overburden pressure from the fill. Jones
87 (2015) highlighted the importance of conducting rigorous geotechnical tests (such as grading
88 analysis, plasticity test and California Bearing Ratio, or CBR, test) to assess the grading coefficient
89 (G_c) and shrinkage product (S_p) of locally available material, which may be incorporated in the
90 design methodology for unpaved roads. Kuttah (2016) emphasized the influence of subgrade
91 moisture conditions and heavily loaded traffic on the performance of gravel roads that can be
92 incorporated in its design methodology. With the aid of the proposed semi-empirical methods
93 (Giroud and Han, 2004; Han and Pokharel, 2015), DACE software® was introduced as a supportive

computational tool for calculating the design thickness of unpaved roads having CBR<3% (Diaz *et al*., 2020).

All the earlier researches carried out on unpaved roads considered the subgrade to be predominantly comprising soft clayey or silty soils. For such saturated subgrades, an undrained condition mostly prevails during the momentary passage of the vehicle. Consequently, to accommodate such worst scenario of undrained analysis, the subgrade resistance was primarily quantified by its undrained shear strength that was correlated to the field CBR value. However, depending on the degree of saturation, permeability and the stratigraphy of the subgrade, the state of drainage can vary (i.e., it may exhibit an undrained, partially drained or fully drained states), which, in turn, would govern the choice of the subgrade strength parameters (effective or undrained strength parameters) and their magnitudes. At the same time, the consideration of purely saturated cohesive medium is mostly idealistic against the realistic prevalence of 'generalized' subgrades that are characterized by both of its shear strength parameters, namely cohesion (c) and angle of internal friction (φ); such soils are also commonly referred as 'c-φ' soils. Owing to inherent higher subgrade strength of the c-φ soils, the application of the conventional design methodology provides an overestimated magnitude of aggregate thickness that might not be practically required. Hence, there is an ardent requirement to improve upon the existing design consideration by incorporating both the shear strength parameters of the generalized subgrade, which would help to attain both safe and economically viable unpaved roads.

In this regard, Meena *et al*. (2013) improvised upon the analytical design methodology proposed by Giroud and Noiray (1981) and produced a pioneering research by considering both the shear strength parameters of subgrade soil to incorporate its bearing resistance in the assessment of the aggregate layer thickness. Such approach revealed recognizable reduction in the aggregate thickness as compared to the outcomes from earlier analytical formulations. However, the traditional limit-equilibrium based analytical formulation (Giroud and Noiray, 1981; Meena *et al*., 2013) did not consider the deformability aggregate and subgrade layers. In such scenario, there were no avenues of assessing the internal stresses and strains developed in different layers of unpaved road due to aggregate and/or wheel loadings. Consequently, the analytical approaches debatably inferred that for stronger subgrades, there would be no requirement of aggregate layer,

while for very weak subgrades, exorbitantly large aggregate thickness would be required. Under the latter condition, the subgrade would not be resisting enough to even bear the weight of the aggregate layer itself during construction and, thus, aggregates would penetrate inside the underlying soft subgrade. Furthermore, it was also considered that the aggregate layer would not fail under vehicular loading. However, in the absence of fine-grained binding material (IRC SP:77, 2008), the stacked unbounded and poorly-graded coarse aggregate would not be mechanically stable to sustain the vehicular loading due to stress concentration at the tire edges. Thus, in a nutshell, as the aggregate and subgrade layers actually deforms under an external load, it is immensely important to assess the performance of an unpaved road under operational conditions.

Thus, considering the deformability of the aggregate and subgrade layers, this paper presents the development of a coupled stress-deformation based design algorithm for unpaved roads in a finite element framework. Although the developed algorithm still confines to the traditional quasi-static design as attempted in earlier researches, at the same time, it improvises upon the same by incorporating the stability of the individual components of unpaved road under all operational conditions (i.e. stability of deformable subgrade under aggregate loading and stability of deformable aggregate under quasi-static vehicular loading).

Numerical Methodology

Description and validation of the FE model

For the present study, FE analysis of an unreinforced unpaved road system is carried out using PLAXIS 2D v2018 numerical modeling software. Figure 1 exhibits a typical geometry of the unpaved road modelled as a two-layered system comprising the overlying aggregate and underlying subgrade layers. The cross-section is considered identical along its longitudinal direction and, hence, the same is represented by a plane-strain model. The lateral boundaries of the subgrade layer are provided with fixities against horizontal displacement, while the bottom boundary is restricted from displacements in any direction. The aggregate layer is modeled as a finite layer over subgrade with sustainable 3H:1V or 4.5H:1V side slopes, such that local slope failure of the aggregate layer can be avoided. Based on the traffic studies that are supposed to be carried out before the actual construction of road, one can ideally ensure a particular value of

155 embankment slope that is to be realistically chosen. Vehicular axle load is applied on the surface
156 of the aggregate layer as a uniformly distributed load at the tire contact area.
157
158 Both the aggregate and the subgrade layers are modeled using linear elastic – perfectly plastic
159 Mohr–Coulomb constitutive model, which uses five parameters; Young's modulus (E) and
160 Poisson's ratio (v) for soil elasticity, while the plasticity is accounted by angle of internal friction
161 (φ), cohesion (c) and angle of dilatancy (ψ) (Lade, 2005). For the present study, dilatancy is not
162 considered. Based on the existing literature and practice, various magnitudes of the strength
163 parameters for the subgrade and the aggregate layer are selected over their suitable ranges
164 (mentioned in appropriate later sections), while the common model parameters (as per Meena *et*
165 *al*., 2013; Yaghoubi *et al*., 2016) are listed in Table 1. These are some typical values of the
166 parameters that falls within the wide range of material parameters and could be reasonably
167 encountered in the construction of such unbounded roads. For the subgrade layer and aggregate
168 layers, the unit weight (γ) is kept same owing to the fact that the unit weight of soil and locally
169 available aggregates are mostly similar and that slight variations in this parameter does not
170 significantly affect the deformation response of the unpaved road system (Meena *et al*., 2013).
171 Based on the strength parameters of aggregate and subgrade, the thickness of the aggregate layer
172 is assessed as per existing analytical solutions (Meena *et al*., 2013).
173

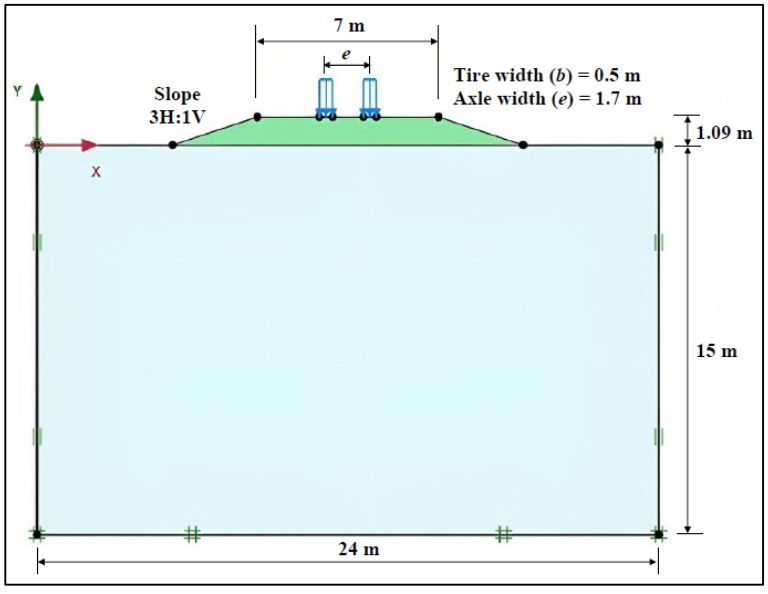

174
175 **Figure 1.** A typical geometry of unreinforced unpaved road

Table 1. Some typical material parameters used in the FE model

Parameters	Subgrade	Aggregate
Constitutive model	Mohr-Coulomb	Mohr-Coulomb
Unit weight (γ) (kN/m^3)	19	19
Elastic modulus (E) (MPa)	20	6
Poisson's ratio (ν)	0.4	0.3

Aided by a robust triangulation scheme with options for global and local mesh refinements, an automatic generation of unstructured 2D finite element mesh of 15-noded triangular elements is used to discretize the model domain. In order to obtain a non-oscillating outcome from the FE analysis, it is important to conduct a mesh quality check and a mesh convergence study to identify the sensitivity of the FE model to the variation in mesh size. In this regard, a mesh convergence study was conducted for a particular model configuration (Figure 2) for three different global meshes, i.e. 'very coarse', 'coarse' and 'medium' respectively, having successively reducing relative mesh sizes. It is noted that beyond the 'medium' mesh size with average mesh element size as 1.25 m, the variation in maximum vertical deformation is negligible, thereby indicating the achieved convergence. Further local mesh refinements are conducted in the areas expecting large stress concentration or large deformation gradients (e.g. aggregate-subgrade interface, corners of the aggregate layer, etc.). Based on the results, Figure 3 shows the optimally discretized model domain assuring best possible symmetry and mesh quality, with an average element size of 0.07727 m.

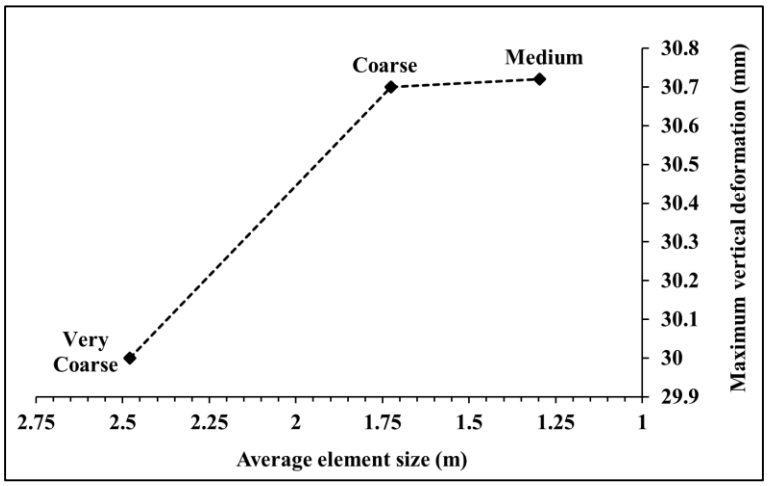

Figure 2. Identification of optimal mesh size from a typical mesh convergence study

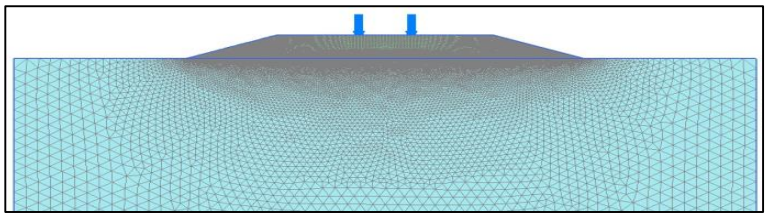

Figure 3. FE discretization and meshing of a typical unreinforced unpaved road geometry

Validation of FE model

A validation study has been carried out to establish the efficacy of the coupled stress-deformation based FE model. Analogically, in terms of the geometry and loading, the FE model adopted for the present study is no different than a problem of interfering surface strip footings resting on two layered media. Hence, for validation, the experimental problem reported by Ghosh and Kumar (2011) is considered in which the footing width (B) is 50 mm, center-to-center spacing of the footing (S) is 3.0B (= 150 mm), and thickness of the top layer (D) is 1.0B (= 50 mm). The angle of friction of the overlying and underlying layers (φ_1, φ_2) are 32.6º and 38.9º, respectively. Based on the remaining information related to the footing material, soil properties, loading conditions and measurement points, the developed FE model is suitably modified. Following the experimental procedure, the load-settlement response obtained from the numerical analysis is compared to that obtained from experimental observation. An appreciable agreement is obtained between the load-settlement responses; the ultimate load obtained from the experimental and numerical exercise is 33 kg and 35 kg, respectively, both corresponding to a settlement value of 6 mm (Figure 4). With the minor dissimilarity within the tolerance limit (<10%), it can be well inferred that the developed FE model is suitably validated for the closely spaced loading representing the dual wheels at the two ends of the axle and the same is considered in the rest of the study.

Coupled Stress-Deformation based Design Methodology for Unreinforced Unpaved Roads

Operational failure conditions and limiting cohesion

As mentioned earlier, the analytical formulations did not address the operational failure conditions, which are presently incorporated in the developed algorithm. In order to counteract the stated operational failures, it is necessary to improve the strength parameters of the aggregate and soil subgrade. In this regard, given the frictional property, the minimum cohesion required individually

by the subgrade and aggregate are determined from limit analysis so that their nominal stability is ensured.

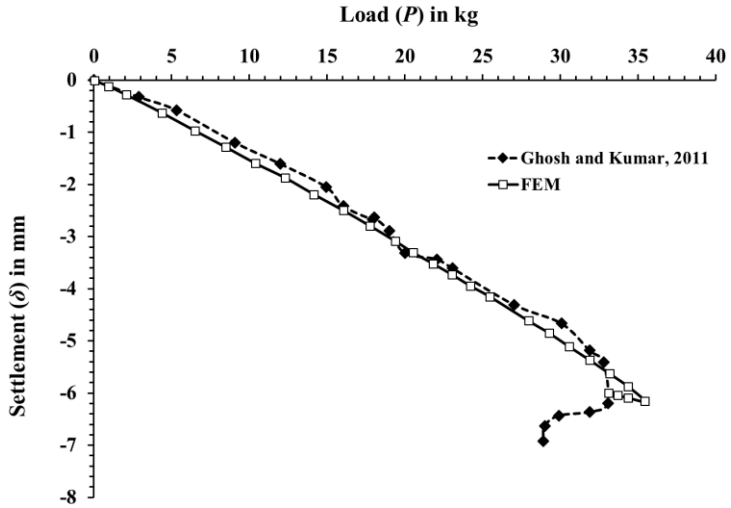

Figure 4. Comparison of the load-settlement response between the experimental and FE results

Limiting cohesion in subgrade layer required to sustain aggregate loading.

The subgrade should be capable enough of sustaining the aggregate load during its placement. Following Terzaghi's bearing capacity formulation for a strip load resting on supporting soil (Terzaghi, 1943), the expression for limiting cohesion has been developed by equating the aggregate load (γh) to the allowable bearing capacity of the subgrade, and is expressed as follows:

$$\gamma h = \frac{c_{s,\min} N_c + 0.5\gamma B N_\gamma}{\text{FoS}} \quad (1)$$

where, h is the height of the aggregate layer, $c_{s,\min}$ is the limiting cohesion required in subgrade to sustain the aggregate loading under operational conditions, and FoS is the safety factor against ultimate bearing strength. The corresponding bearing capacity factors (N_c, N_γ) are to be determined based on the friction angle of the subgrade material (Terzaghi, 1943). If the subgrade already possesses cohesion more than the limiting magnitude, then this assessment would not be required.

Limiting cohesion in aggregate layer required to sustain quasi-static vehicular loading.

The aggregate layer having poor bearing strength can fail under punching shear due to the imposed quasi-static vehicular load. For preventing such punching failure, the stress concentration under

edges of the tire contacts should be dispersed to a magnitude lower than the allowable bearing capacity of the aggregate alone. The equilibrium of the same can be expressed as:

$$\frac{P}{2lb} = \frac{c_{a,\min} N_c + 0.5\gamma b N_\gamma}{\text{FoS}} \quad (2)$$

where, P is the axle load, l and b are the dimensions of the equivalent contact area of the dual wheel system on aggregate layer (Giroud and Noiray, 1981), and $c_{a,\min}$ is the limiting cohesion required to prevent punching shear failure in the aggregate layer due to the imposed quasi-static vehicular loading. The corresponding bearing capacity factors are to be determined based on the friction angle of the aggregate material. It may be noted here that addition of fines in the aggregate layer would require additional attention to the drainage behavior of the aggregate; however, the same is beyond the scope of the reported work.

Additional cohesion requirement of subgrade considering deformability of aggregate and subgrade.

The earlier sub-sections described the necessity to evaluate the minimum strength parameters required by the subgrade and aggregate to ensure their individual operational stability against failure. The subgrade stability was ensured solely against the aggregate placement, while the aggregate stability was ensured solely under the vehicular load considered it to be resting on a non-deformable subgrade. However, in practical scenario, the stress-deformation mechanism of the unpaved road system will be coupled and the subgrade would be a deformable medium; thereby, the stability of subgrade and aggregate layers would be affected by the stress-deformation interaction between the layers. Thus, even after achieving independent operational stability based on the assumptions of non-deformability of individual components, once the aggregate layer is strengthened, additional stress from vehicular loading gets transferred to the subgrade that was not considered when the subgrade was strengthened only to sustain the placement of aggregate layer. This additional stress passes to the subgrade through stress-deformation mechanism at aggregate-subgrade interface and is primarily observed when aggregate layer is subjected to vehicles with high axle-loads. This additional stress is termed a ‘secondary stress’ and needs to be taken into account in the design to ensure the overall stability of the subgrade. Hence, when such a situation is encountered, the cohesion of the subgrade needs to be further readjusted to arrive at a modified minimum value ($c_{sa,min}$) that would render the subgrade enough bearing strength to sustain the

overall imposed stress. Further details about the descripted procedure is provided in the next section.

Detailed design methodology

The following section provides a step-by-step procedure to be adopted for the design of unreinforced unpaved roads through a coupled stress-deformation based approach as proposed in the present study employing FE analysis.

Step 1. Make a preliminary assessment of the required aggregate thickness based on the analytical expression developed by Meena *et al.* (2013).

Step 2. Develop the FE model in PLAXIS 2D using aggregate thickness assessed in Step 1. The shear strength parameters ($c_{subgrade}$, $\varphi_{subgrade;}$ and $\varphi_{aggregate}$) for subgrade and aggregate layers is to be kept same as that used in Step 1 for assessing the aggregate thickness. The values of other model parameters such as modulus of elasticity (E), Poisson's ratio (ν), unit weight (γ) and initial void ratio (e_{init}) are adopted as per field specifications.

Step 3. The simulation of the FE model developed in Step 2 is undertaken to investigate the operational instability of the subgrade solely due to aggregate loading. If the operational stability is not jeopardized, consider $c_{s,min}$=$c_{subgrade}$ and continue to Step 6. If the FE model exhibits stress-based failure in the subgrade, continue to Step 4.

Step 4. Assess the limiting magnitude of cohesion ($c_{s,min}$) required in the subgrade layer (as per Eqn. 1) to sustain the operational aggregate loading.

Step 5. Using the $c_{s,min}$ value obtained in Step 4, analyse the FE model developed in Step 2 to ascertain the operational stability of the subgrade under aggregate loading. If the subgrade remains stable under the aggregate load, continue to Step 6. If the subgrade still portrays failure, repeat Step 4 to re-estimate $c_{s,min}$ with increased FoS.

Step 6. Reform the FE model by incorporating $c_{s,min}$ as the cohesive parameter for the subgrade (obtained in Step 5) over and above the friction parameter of the subgrade ($\varphi_{subgrade}$). Investigate whether the aggregate layer (with strength parameter adopted in Step 1 or Step 2) is operationally stable and able to sustain the stress concentration imposed by the quasi-static vehicular load against punching shear failure.

Step 7. If operational stability of aggregate layer is ensured, the design of unpaved road is deemed complete with $\varphi_{subgrade}$ and $c_{s,min}$ as the shear strength parameters for the subgrade, and $\varphi_{aggregate}$ as the shear strength parameter for the aggregate.

Step 8. If the aggregate fails under the imposed vehicular load, determine the minimum value of cohesion required ($c_{a,min}$) in the aggregate using Eqn. 2.

Step 9. Analyse the reformed FE model developed in Step 6 (already having $\varphi_{subgrade}$, $c_{s,min}$ and $\varphi_{aggregate}$) by incorporating $c_{a,min}$ as limiting aggregate cohesion to reassess its operational stability.

Step 10. If the aggregate still exhibits operational instability, considering a higher FoS. Further, proceed to Step 9 to include the re-estimated $c_{a,min}$ in the reformed FE model that is already incorporating the $\varphi_{subgrade}$, $c_{s,min}$ and $\varphi_{aggregate}$ (from Step 6). If the reformed FE model with higher magnitude of $c_{a,min}$ in aggregate layer exhibits operational stability, proceed to Step 11; else, repeat Step 10 again by heuristically and iteratively enhancing $c_{a,min}$ to a higher value.

Step 11. If the aggregate does not exhibit stress-based failure under imposed load and that the operational stability of the aggregate is ensured, the strength parameters of unpaved road system is finalized to $\varphi_{subgrade}$ and $c_{s,min}$ as the shear strength parameters for the subgrade, along with $\varphi_{aggregate}$ and $c_{a,min}$ as the shear strength parameter for the aggregate. Further, it is necessary to check whether the reformed FE model exhibits failure in the subgrade due to such secondary stresses generated from simultaneous aggregate and vehicular loading. Following this principle, the unpaved road system is further checked for failure under secondary stresses.

Step 12. If no secondary stress-based failure is noticed, the design of unpaved road system is deemed complete with the strength parameters finalized and mentioned in Step 10.

Step 13. Any instability in the subgrade arising due to the secondary stresses (as in Step 11) can be tackled by heuristically and iteratively increasing the value of $c_{s,min}$ to a modified higher value ($c_{sa,min}$).

Step 14. The FE model is reanalysed with $c_{sa,min}$ as subgrade cohesion to reconfirm the stability of the system.

Step 15. If the stability against secondary stresses is achieved, the design of unpaved roads is deemed complete with the strength parameters of unpaved road system is finalized to $\varphi_{subgrade}$ and $c_{sa,min}$ as the shear strength parameters for the subgrade, along with $\varphi_{aggregate}$ and $c_{a,min}$ as the shear strength parameter for the aggregate. If the stability is yet to be achieved, repeat from Step 13.

For easy visual perception, the described coupled stress-deformation based design methodology of unreinforced unpaved roads is illustrated through a flowchart in Figure 5. It is to be noted that any type of strength enhancement of the subgrade calls for ground improvement techniques (Miekos *et al*., 2019; Georgees and Hassan, 2022; Magalhaes *et al*., 2022; Pooni *et al.*, 2023). The effective depth of such improvement in the subgrade can be identified based on the extent of strain concentration zone within the subgrade. With regard to the strength enhancement of aggregate, mixing of fines with the aggregate material is the most viable solution (Thogersen *et al.*, 2013; Barbieri *et al.*, 2019, 2020; Lopez-Uceda *et al*., 2020; Freira *et al*., 2021; Ramdas *et al.*, 2021). However, the entire context of ground improvement and aggregate strengthening techniques is beyond the scope of present study.

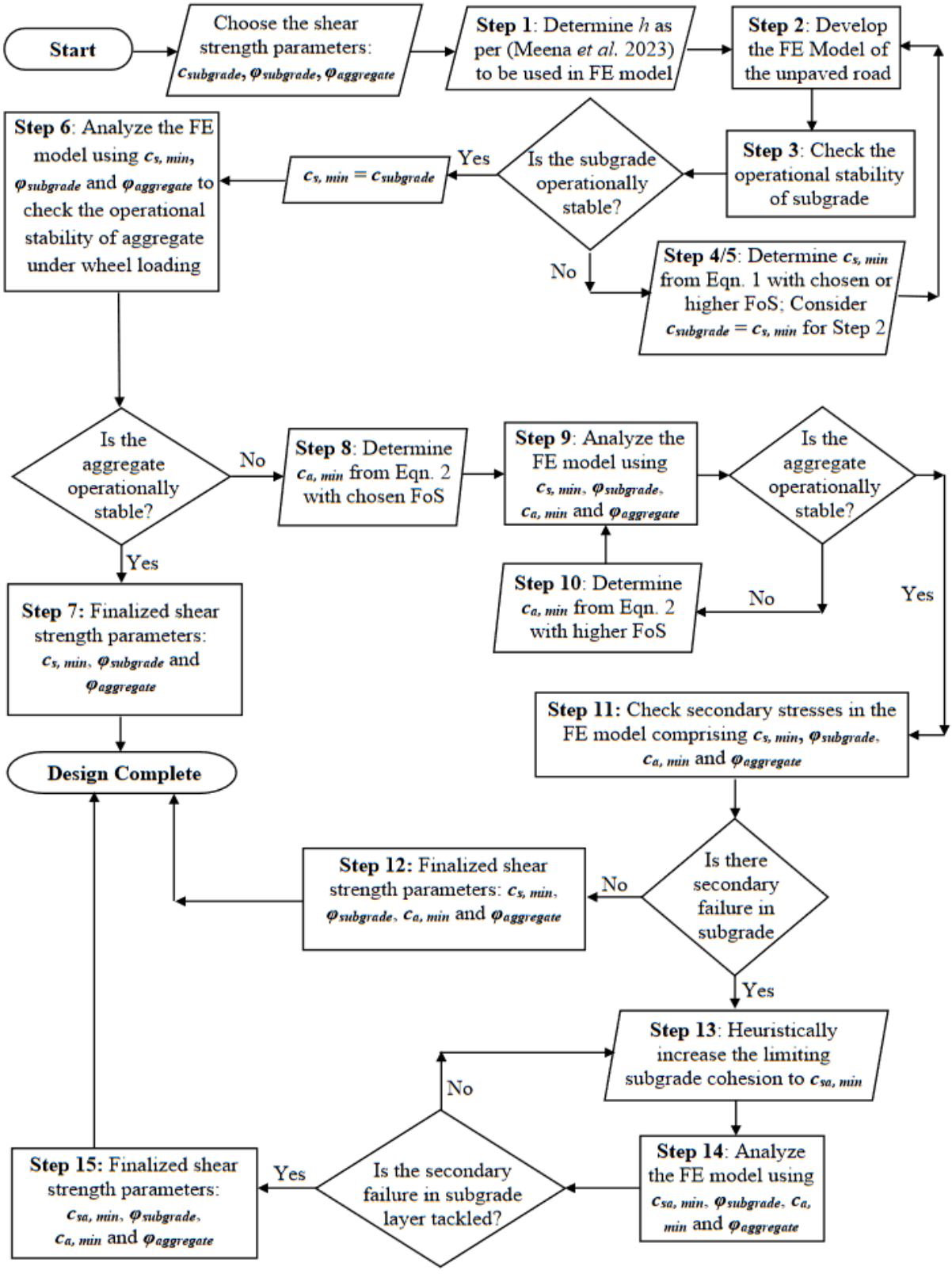

Figure 5. Flowchart of proposed stress-deformation based design algorithm for unpaved roads

Validation of the Developed Algorithm

For any developed design algorithm, a validation study is required to ensure the proper application of the methodology in real field scenario. In this regard, for validating the coupled stress-deformation based design algorithm developed in the present study, the large-scale experimental work reported by Poorahong *et al.* (2024) involving a fully instrumented unpaved road model constructed on soft clay subgrade is considered. The experimental unpaved road structure comprised a crushed rock aggregate layer resting on a soft clay subgrade layer. The unpaved road model was designed to support standard axle load of 80 kN with tire pressure set at 550 kPa, thereby leading to a tire contact dimensions of 0.38 m × 0.27 m (Dey and Meena 2013; Meena *et al.*, 2013). The California Bearing Ratio (CBR) of the aggregate and subgrade layer is provided as 80% and 4%, respectively (Poorahong *et al.*, 2024). Accordingly, undrained cohesion of the individual layers of the unpaved road model is determined using the correlation $c_u\left(\text{kPa}\right) = 30\ (\text{CBR in \%})$ as proposed by Giroud and Noiray (1981), which comes out to be 2400 kPa and 120 kPa, respectively. Since the soft clay subgrade is represented with undrained cohesion, the bearing capacity factors are considered for a $\phi = 0$ condition that comes out to be $N_c = 5.7,\ N_q = 1$ and $N_\gamma = 0$ (Terzaghi, 1943). The unit weights of the aggregate and subgrade layers are given as 22 kN/m^3 and 17.8 kN/m^3, respectively. Based on the parameters ascertained for the unpaved road model, the preliminary assessment of the aggregate thickness is carried out as per Step 1 of the algorithm. It is noted that a nominal aggregate cover of 0.15 – 0.2 m can be provided (Sarma and Dey, 2024a, 2024b). The thickness of the crushed rock aggregate layer used in the experiment is 0.2 m, which conforms to the assessment from the developed algorithm. Following the design methodology, the FE model of the unpaved road is designed. Firstly, as per Step 3 of the design algorithm, the operational stability of the subgrade under base layer loading is checked, in which the subgrade is found to be operationally stable. This conformed to the experimental observation that the subgrade did not exhibit failure under placement of the aggregate layer. Further, as per Step 8, the operational stability of crushed stone base layer is checked under the vehicular load placement is checked, in which it is found to be operationally stable as no punching shear failure was noticed within the aggregate layer. The same was noticed in the experimental program, in which it was noticed that under the vehicular loading, the failure pertained to the local shear failure. Hence, the design algorithm developed in the present study suitably determined the stability of the unpaved road section as determined in the experimental program by Poorahong *et al.* (2024). In this regard, the performance of the recognized design section was ascertained through a load deformation response of the unpaved road when subjected to the stated vehicular load. Figure 6 shows the comparison between the FE results and experimental results, that exhibits appreciable agreement in the trend and magnitudes of bearing pressure and settlement.

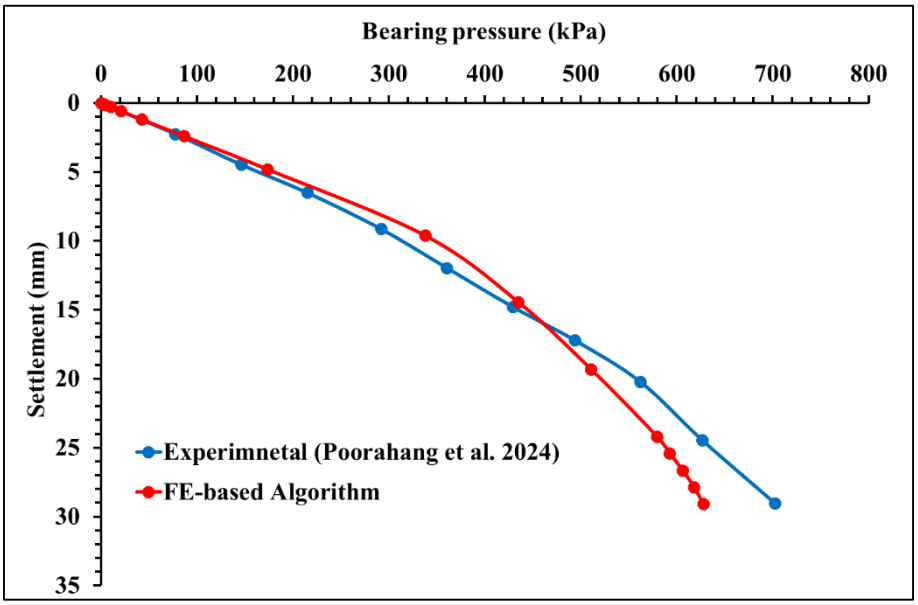

Figure 6. Comparison of bearing pressure vs settlement response between the experimental and FE results for the unreinforced unpaved road

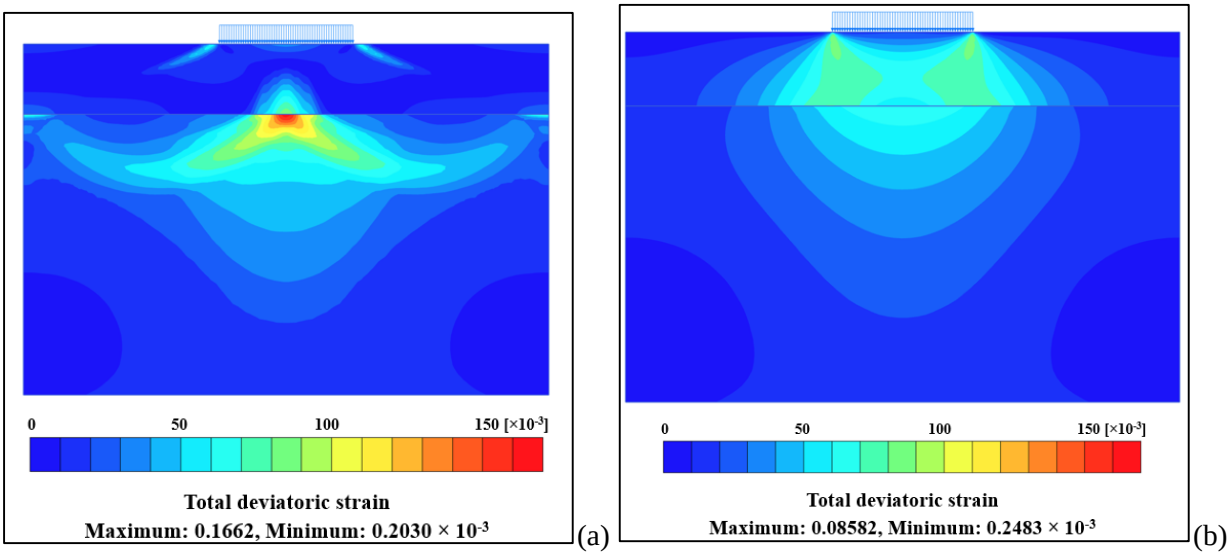

Figure 7. (a) Development of secondary stresses in the subgrade due to combined aggregate and vehicular loading (b) Arresting of the developed secondary stresses within the aggregate layer by heuristically increasing the strength parameter of the subgrade equal to that achieved by geogrid-reinforced unpaved road section

Under this scenario, as per Step 11, the secondary stresses in the subgrade are ascertained. It is noted from Fig. 7a that significant secondary stresses are generated in the subgrade layer due to combined loading of the aggregate and vehicular loading. In further tests conducted by Poorahong *et al.* (2024) using a geogrid layer at the interface of base layer and subgrade layer, the bearing capacity increases to approximately to 1040 kPa. This implies at this particular value, the geogrid has captured the deviatoric strains within the aggregate layer when subjected to combined aggregate and vehicular loading. As an analogy, following the Step 13 of the developed design algorithm, the necessary ground improvement required for unreinforced unpaved road is addressed by heuristically increasing the undrained strength of the subgrade layer to a value of 1000 kN. The corresponding deviatoric strains are shown in Figure 7b, which essentially shows that the deviatoric strains are captured within the base-subgrade interface. With these above mentioned conformation to the large-scale experimental tests conducted by Poorahang *et al*. (2024) to assess the bearing capacity of an unpaved road structure (comprising crushed rock aggregate layer resting on soft clay subgrade) when subjected to standard vehicle axle load, the 'stress-deformation based algorithm for quasi-static designing unreinforced unpaved roads incorporating operational stabilities' stands validated.

Results and Discussions

Outcomes from a typical FE-based simulation involving $c_{s,min}$ and $c_{a,min}$

Several FE models were developed with different combinations of parameters, namely axle load (P), tire pressure (P_c), cohesion of subgrade ($c_{subgrade}$), angle of internal friction of soil ($\varphi_{subgrade}$), angle of internal friction of aggregate ($\varphi_{aggregate}$) and Factor of safety (FoS). However, only one typical model is highlighted here to illustrate the various outcomes and inferences from the FE-based design methodology. The parametric values for the parent model considered herein are P = 30 kN, P_c = 600 kPa, $c_{subgrade}$ = 1 kPa, $\varphi_{subgrade}$ = 5° and $\varphi_{aggregate}$ = 35°. Based on the chosen axle load and tire pressure, b is obtained to be 0.27 m. A FoS = 1.5 is used for the analysis. Through this consideration, the subgrade is considered to be sufficiently weak so that all the steps of the FE-based design methodology could be highlighted. The design steps and their outcomes are described as follows:

- **Step 1**: Based on the given data and using the analytical expression developed by Meena *et al.* (2013), the aggregate thickness (h) is preliminarily assessed to be 0.98 m.

- **Step 2**: A finite element model is designed with the assessed thickness of aggregate layer having side slopes adjusted to 3H:1V to prevent any unwarranted slope failure. Figure 8 shows the typical FE model wherein the subgrade layer is subjected to aggregate loading.

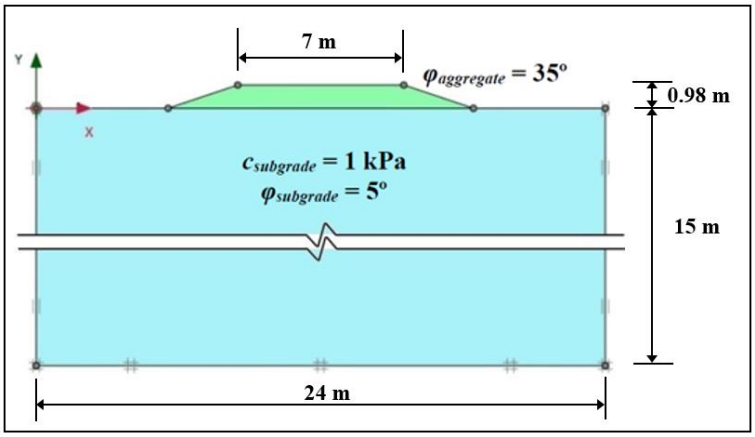

Figure 8. FE model of unpaved road with subgrade subjected to aggregate loading

- **Step 3**: In this step, the operational stability of the subgrade under the aggregate loading (as mentioned in Step 2) is checked through the total and incremental deviatoric strain diagrams. The total deviatoric strain diagram portrays deviatoric strain accumulated at the end of successive calculation steps (at the end of each load-stepping procedure) when the stress-deformation problem is being solved. The incremental deviatoric strain is the differential deviatoric strain calculated between latest and the preceding load-step. The incremental deviatoric strain distinctively highlights the strain concentrations at the end of each load-step, which are represented as slip lines. Successive representation of these diagrams elucidates the evolution of potential failure lines during the simulation. Figure 9a and 9b clearly show the distinct development of strain concentration zones and the development of slip lines through the aggregate layer and propagating to the subgrade layer. The output results imply that in contrary to the assumptions of the analytical model, the subgrade is not sufficiently strong to bear the aggregate loading and that it would fail even due to the laying of the aggregate, thereby necessitating a ground improvement technique to enhance its strength properties. It can be noted that the developed strains are not confined to the side slopes of the aggregate, rather they are penetrating considerably within the subgrade through the aggregate-subgrade interface. Thus, it is not a simple side-

slope failure in the aggregate, rather the subgrade is failing due to the concentration of strains originating due to aggregate loading. The failure region is also noticeably marked by stress concentrations that are indicated through the development of plastic points as shown in Figure 9c. Plastic points are the locations which exhibit complete or nearly-complete mobilization of the shear strength of soil at that location. It can be noted that the plastic points are densely spread in the aggregate, and a significant accumulation takes place in the subgrade beneath the aggregate. From all these observations, it is clear that with the typical basic parametric set considered herein, the subgrade undergoes failure even under the aggregate loading. This phenomenon is not reflected in the analytical estimation of the aggregate thickness. This observation, highlighted by the coupled stress-deformation approach, necessitates the stabilization of the subgrade to achieve an enhanced strength in order to sustain the operational stability under aggregate loading.

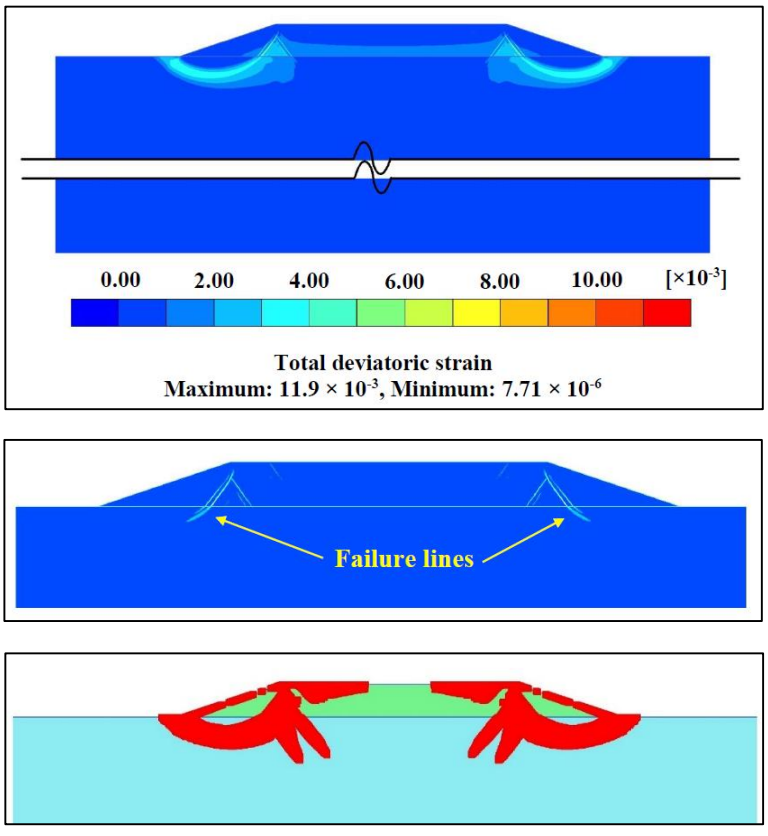

Figure 9. Strain-deformation response of subgrade subjected to aggregate loading considering basic parametric set as obtained from analytical modeling: (a) Total deviatoric strain shading (b) Incremental deviatoric strain shading (c) Plastic point distribution

- **Step 4**: It is established in Step 3 that enhancement of subgrade strength is required. In this regard, to maintain the operational stability, the minimum cohesion ($c_{s,min}$) required in the subgrade layer to sustain the aggregate loading is assessed (as per Eqn. 1) to be 3.65 kPa, which is more than the previous value of $c_{subgrade}$ = 1 kPa. It is to be noted that any ground improvement method adopted would also increase the friction angle of the modified subgrade. However, in this study, only the increment in cohesion is considered, thereby rendering the design to feasibly conservative.

- **Step 5**: Using the modified subgrade cohesion $c_{s,min}$, the FE model is further analysed. Under this scenario, the aggregate-subgrade system did not exhibit any failure, thereby proving the sufficiency of the improved subgrade strength considered in the analysis. Figure 10 shows the total deviatoric strain diagram and the plastic point distribution developed in the system. It can be noted that the strains are well captured and restricted within the aggregate layer, while the plastic points diminished significantly in comparison to what was noted in Figure 9c. It is to be noted that increase in the subgrade cohesion substantially arrested the internal deformation within the unpaved road system under aggregate laying scenario, thereby distinctively highlighting the formation of plastic points throughout the unconfined free surface of the aggregate layer in Figure 10b, and is not related to a real rupture. Plastic points are expectedly observed only on the free surface of the deformable cohesionless aggregate. After incorporating $c_{s,min}$ value, it is found from Figure 10a that the maximum magnitude of total deviatoric strain is 1.497×10^{-3}, which is almost 8 times lesser than the maximum value of 11.9×10^{-3} obtained in Step 3. These observations conclusively indicated that the subgrade system with improved strength parameters (as estimated in Step 4) is capable of bearing the aggregate load and would not fail under this particular phase of operation. This step reenacts the necessity to depend on coupled stress-deformation based finite element modeling to assess the operational response of subgrade under aggregate loading.

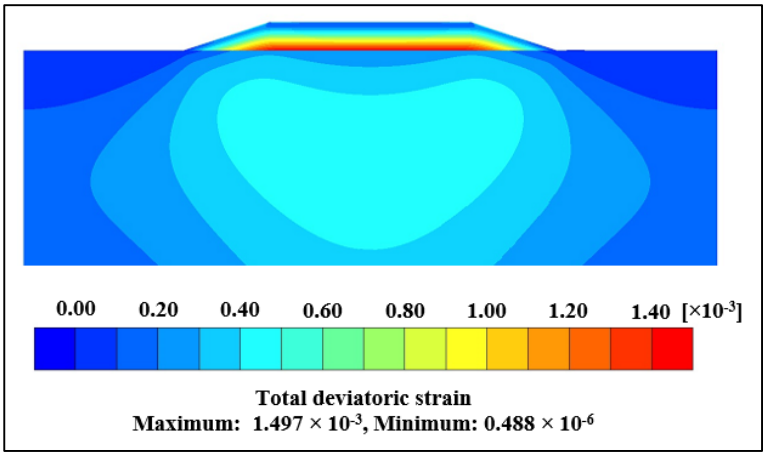

(a)

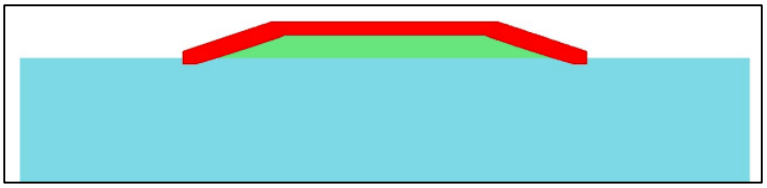

(b)

Figure 10. Response of subgrade subjected to aggregate loading considering the improved strength parameter of subgrade: (a) Total deviatoric strain (b) Plastic point distribution

- **Step 6**: Further, the quasi-static vehicular load is applied on to the aggregate layer resting on the reformed subgrade, as shown in Figure 11, and the corresponding responses are studied. Under vehicular load, it is noted that the FE model simulation exhibited failure.

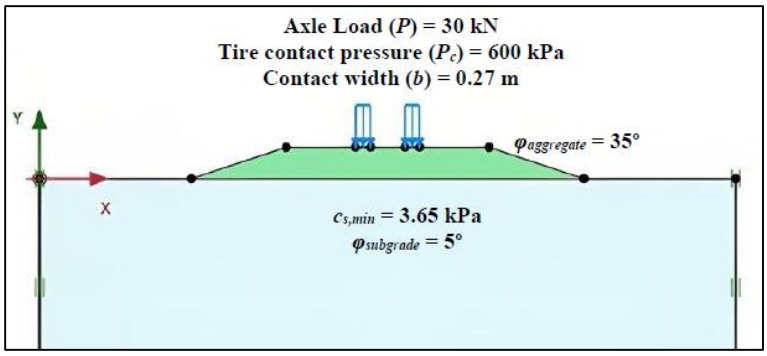

Figure 11. FE model of unreinforced unpaved road subjected to vehicular load

Figure 12a shows the total deviatoric strain diagram under the point of applications of quasi-static wheel loads. It can be observed that the strains are heavily concentrated within the aggregate and closer to the free surface. A closer view shows that the strain

concentration is maximum beneath the edges of the wheels, having a substantially high value of $214x10^{-3}$. This is a distinct indication of the development of punching shear failure mechanism within the aggregate layer due to the imposed wheel load. It can also be noticed that the failure lines develop from beneath the edges of the wheel remain confined within the aggregate layer and do not propagate all the way down to the subgrade layer. Figure 12b exhibits the total major principal strains developed under the wheel loading. It can be noticed that the significant strains have developed in the aggregate layer, and the developed strains are well restrained within the aggregate-subgrade interface. Figure 12c exhibits the development of shear stress concentrations beneath the wheels. Based on the overall observation, it is understood that the strength of the chosen aggregate is insufficient to prevent punching failure of the aggregate subjected to the considered wheel stresses. Hence, there is a necessity to improve the aggregate strength in order to bear the wheel stresses and maintain the operational stability of the aggregate layer.

- **Step 8**: In order to tackle the punching shear failure scenario in the aggregate layer as highlighted in Step 6, the shear strength of aggregate needs to be improved by the addition of fines in the aggregate layer. For the present problem, using Eqn. 2, the minimum value of cohesion required ($c_{a,min}$) in the aggregate is determined to be 12.77 kPa, which is supposed to ensure the operational stability of the aggregate layer while sustaining the quasi-static wheel load.

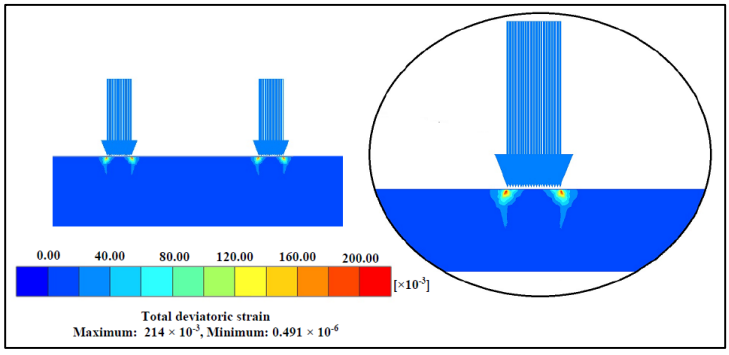

(a)

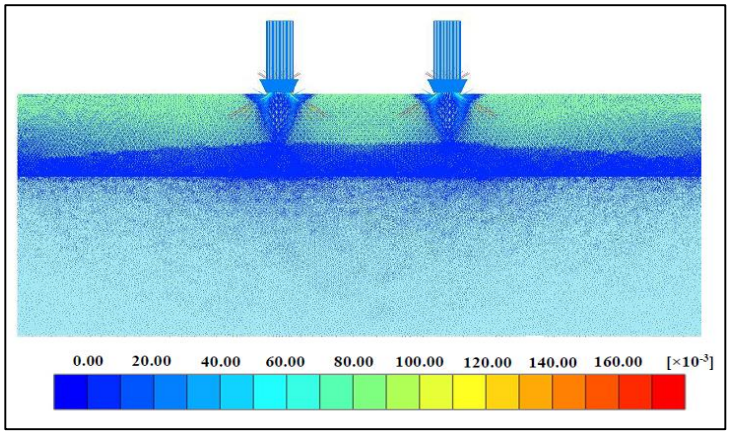

(b)

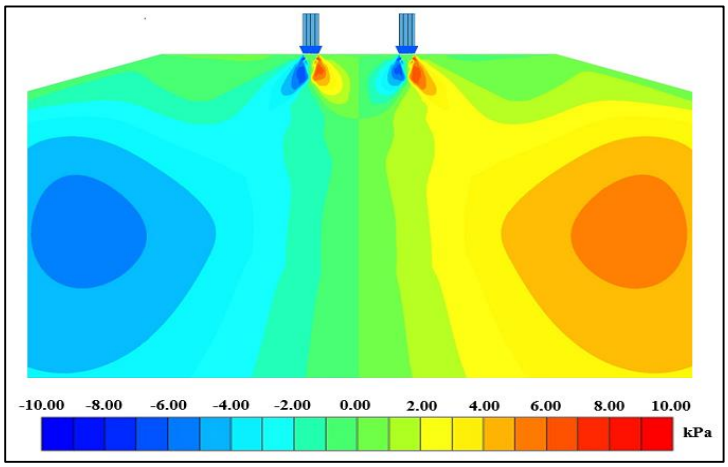

(c)

Figure 12. Response of the FE model of unreinforced unpaved road with basic strength parameters of aggregate layer and subjected to vehicular load (a) Total deviatoric strain (b) Total major principal strain and (c) Cartesian shear stress distributions

- **Step 9**: Using the modified cohesion value of aggregate ($c_{a,min}$), the FE model developed in Step 6 is further analysed. Figure 13 shows the total deviatoric strain diagram for the particular case, which clearly highlights that the strains are distributed evenly to a larger area, successively from wheel to aggregate and then to the subgrade. The maximum strain developed is obtained as 6.74×10^{-3}, which is almost 30 times less than the maximum strain value obtained in Step 6 (i.e. 214×10^{-3}).

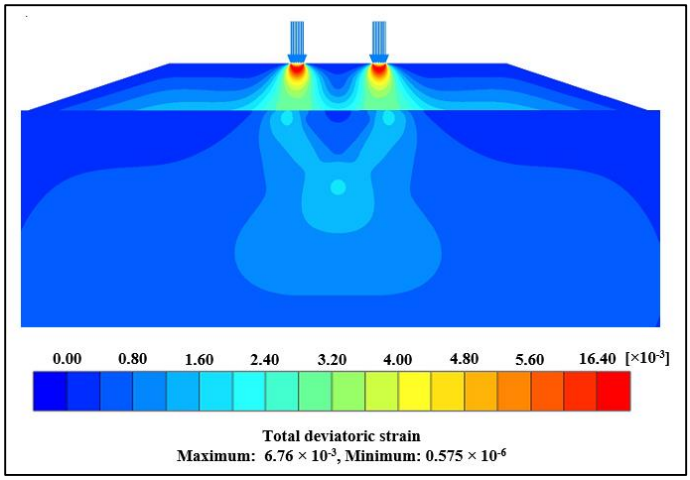

Figure 13. Response of subgrade subjected to vehicle loading considering the improved strength parameter of aggregate in terms of total deviatoric strain developed in the system

- **Step 11:** Thus, based on these observations, it is concluded that the modified aggregate strength, demarcated by the usage of minimum cohesion $c_{a,min}$ in the aggregate layer, is effective in maintaining the operational stability of the aggregate layer and prevent punching shear failure under the quasi-static vehicular load. In regard to the model parameters chosen for this exemplification, there is no noticeable secondary stresses developed in the subgrade due to the deformation of the strengthened aggregate layer. Yet, there might be situations when the subgrade layer succumbs to a failure even after the strength improvement of the aggregate layer due to the development of secondary stresses, which would be highlighted in the next example.

- **Step 12 / Final step**: The limiting cohesion of the subgrade and the aggregate layers ($c_{s,min}$ and $c_{a,min}$: obtained from Step 4 and Step 8, respectively), along with their corresponding friction angles, are considered to be the final strength parameters for this particular configuration of unpaved road system.

Outcomes from a typical FE-based simulation involving $c_{s,min}$, $c_{a,min}$ and $c_{sa,min}$

This example highlights the design steps associated with the situation when secondary stresses develop in the subgrade layer after strengthening of the aggregate layer to satisfy its operational stability. Such a situation is expected when higher axle loads are to be supported by the unpaved

road. Under such a scenario, even after adopting limiting strength parameters ($c_{s,\,min}$ and $c_{a,\,min}$) to suffice the operational stability, further strength improvement of the subgrade would be necessary. In this regard, as an exemplification, a higher axle load (as compared to that adopted in previous case) is chosen for the present case, and a model configuration is chosen as follows: P = 80 kN (Standard axle load), P_c = 600 kPa, b = 0.37 m, $c_{subgrade}$ = 1 kPa, $\varphi_{subgrade}$ = 5° and $\varphi_{aggregate}$ = 25°. For the sake of brevity, Steps 1-7 are not reiterated further, as it follows the same suit as discussed in previous case. For this chosen configuration, the additional limiting cohesion required in the subgrade ($c_{s,min}$) and aggregate ($c_{a,min}$) layers are obtained as 1.82 kPa and 15.56 kPa, respectively. Further detailing to illustrate the stated issue is discussed from Step 11 onwards.

- **Step 11**: The FE model incorporating $c_{s,min}$ and $c_{a,min}$ is analysed. In contrary to the observation at this same step made in the previous section, the current FE model with higher axle stresses exhibited further failure, as illustrated in Figure 14. It is to be remembered that the subgrade was already strengthened a-priori to support the operational aggregate loading. However, as the aggregate layer is further strengthened to arrest the strains within the layer (and to prevent punching from heavier axle loads), more stresses (generated due to higher axle load) eventually gets transmitted towards the subgrade, thereby leading to secondary stress concentration within the subgrade. Since the subgrade was not initially strengthened to sustain this unforeseen additional stress below the aggregate-subgrade interface, a secondary failure of the aggregate-subgrade system is experienced. Figure 14a exhibits a high deviatoric strain (14.81×10^{-3}) accumulated below the aggregate-subgrade interface. Further, a distinct migration of strain concentration from the aggregate to the subgrade through their interface can be clearly noted with the aid of a total principal strain diagram, as in Figure 14b. With the aid of incremental deviatoric strain diagram for this particular configuration (as shown in Figure 14c), consequential development of the slip lines within the subgrade can be clearly noticed, thereby indicating the bearing capacity failure of the subgrade with recognizable demarcations of the failure zones (as generally noticed in the Terzaghi's bearing capacity failure problem for shallow foundation systems). A reconciling observation is made from the accumulation of plastic points (as shown in Figure 14d). It can be clearly noticed that the plastic points trace the

shear stress yielding from beneath the wheel contacts in the aggregate layer and, further, get distributed over a wide region beneath the aggregate-subgrade interface.

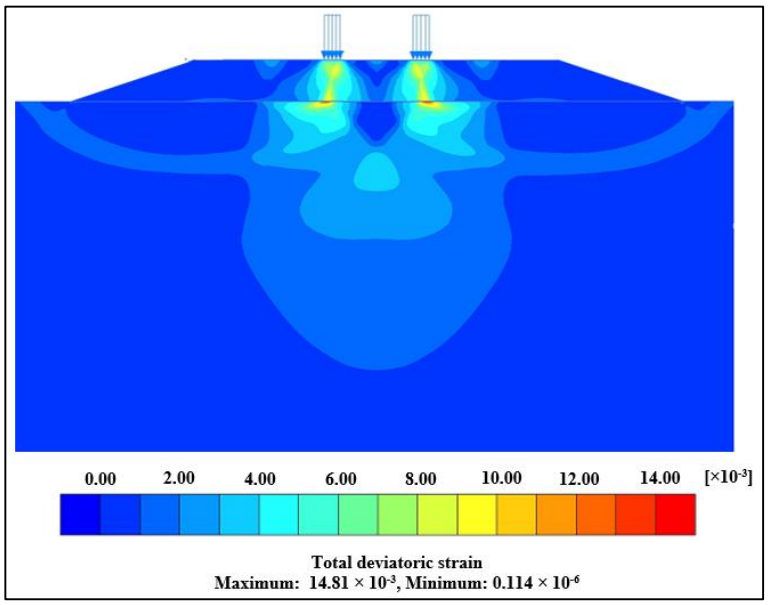

(a)

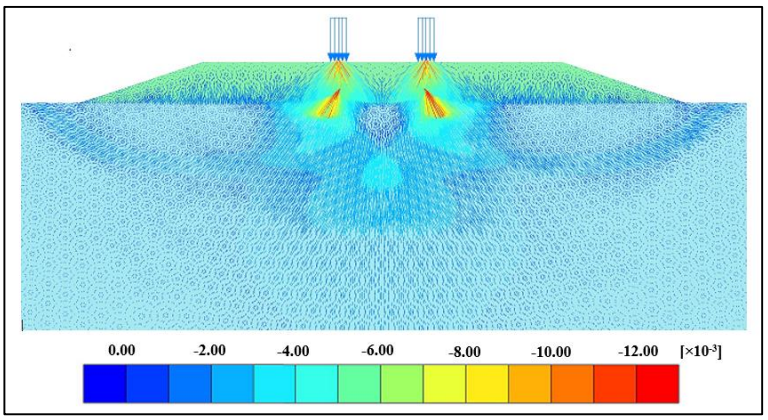

(b)

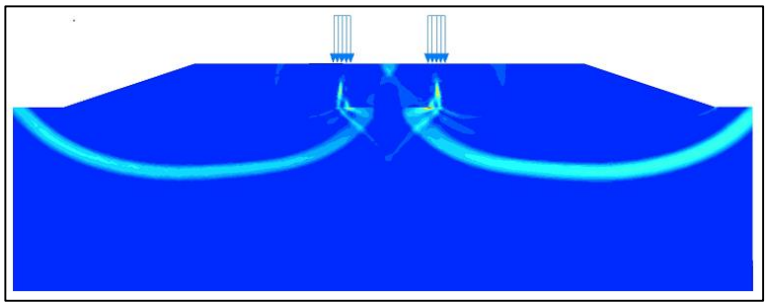

(c)

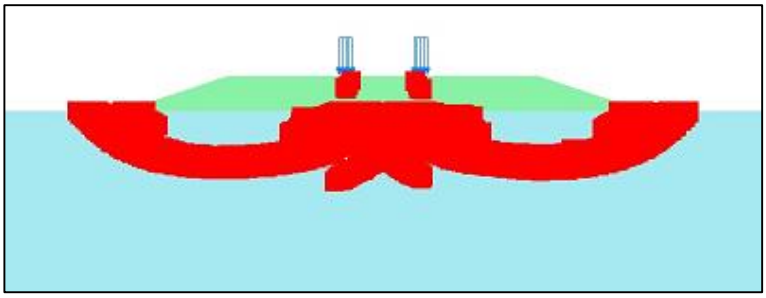

(d)

Figure 14. Response of the aggregate-subgrade system subjected to higher axle load after strength improvement of the aggregate layer: (a) Total deviatoric strain (b) Principal strain (c) Incremental deviatoric strain (d) Plastic points

An additional attempt is made by further strengthening the aggregate layer to investigate if it would prevent secondary failure of the subgrade. In this context, a higher FoS of 1.5 is considered, and the $c_{a,min}$ value is assessed to be 24.01 kPa. This modified $c_{a,min}$ value is used along with $c_{s,min}$ value of 1.81 kPa to analyse the model for obtaining its response. Even this attempt with modified strength parameters exhibits a failure in the unpaved road section, with no decipherable changes in the maximum deviatoric strain and slip lines (the contour diagrams are omitted here for the sake of brevity). These observations reinforce the understanding that with higher axle loads, the failure in the subgrade is mainly governed by the secondary stresses transferred to the subgrade due to the strengthening of the aggregate layer (as ideated earlier). Hence, in this circumstance, further strengthening of the subgrade layer would be necessary.

- **Step 13**: From Step 11, it is clearly understood that the shear strength of subgrade, that satisfied its operational stability, remains insufficient to bear the transmitted secondary stresses. This is dealt by iteratively and heuristically increasing the value of $c_{s,min}$ to an enhanced value ($c_{sa,min}$) to cater the secondary stresses at the aggregate-subgrade interface. Hence, for the next level of analysis of managing secondary stresses in the subgrade, the $c_{s,min}$ is increased from 1.82 kPa to 3.5 kPa.

- **Step 14:** The reformed FE model is analysed with $c_{sa,min}$ of 3.5 kPa. It is found that the simulated FE model did not exhibit further failure; therefore the enhanced $c_{sa,min}$ becomes

caters the modified subgrade shear strength parameters, thereby rendering it sustainable under various operational conditions (stresses from aggregate loading as well as secondary stresses quasi-static wheel load on a strengthened aggregate layer).

Figures 15 and 16 represent the improvement in the response of the aggregate-subgrade system due to the strength improvement of the subgrade soil considering two different $c_{s,min}$ values, 2 kPa and 3.5 kPa. It can be noted that even minor enhancements in the strength parameters profoundly affects the response of unpaved road system. Figure 15 highlights the total displacement diagrams that reveal a significant reduction in displacement from 169 mm to 29 mm even with a nominal increment in $c_{s,min}$ from 2 kPa to 3.5 kPa. Similar observation is made from the total deviatoric strain diagrams (Figure 16), which shows a reduction in the corresponding maximum magnitudes from 810×10^{-3} to 39×10^{-3}. Apart from the declining magnitudes, it can also be noted that the failure mechanism also undergoes a recognizable change with the increment in the subgrade cohesion. For subgrade cohesion $c_{s,min}$ = 2 kPa, distinct development of the slip lines, analogous to a general shear failure condition, is noticed in the subgrade (Figure 16a). It can be noted that the deviatoric strains are concentrated beneath the wheels (due to a strengthened aggregate layer), while the same spreads over large area below the aggregate-subgrade interface as well. The failure lines extend beyond the toe of side slopes, thereby clearly indicating the possibility of the extended failure of the unpaved road system along the entire width of the aggregate mound. This scenario is an extreme detrimental case which should be avoided at all conditions. On the other hand, when the subgrade cohesion was increased to be $c_{sa,min}$ = 3.5 kPa, a significant transition in the evolution of the failure mechanism is noticed. Figure 16b shows a more unified and uniform distribution of the total displacement contours, indicative of a uniform stress transfer mechanism through the aggregate-subgrade interface. Further, Figure 16b also exhibits that the total deviatoric strains are diffused and considerably restrained below the aggregate-subgrade interface and is confined within the central portion of the aggregate-subgrade system. This is indicative of a distinct restrain on the spread of the failure mechanism by controlling the cohesion of the subgrade.

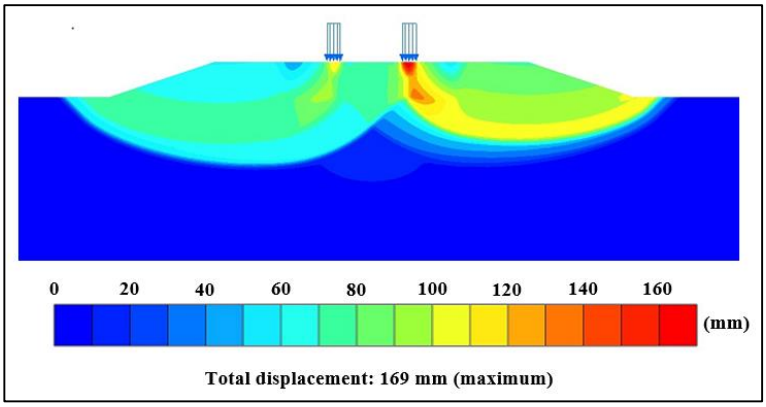

(a)

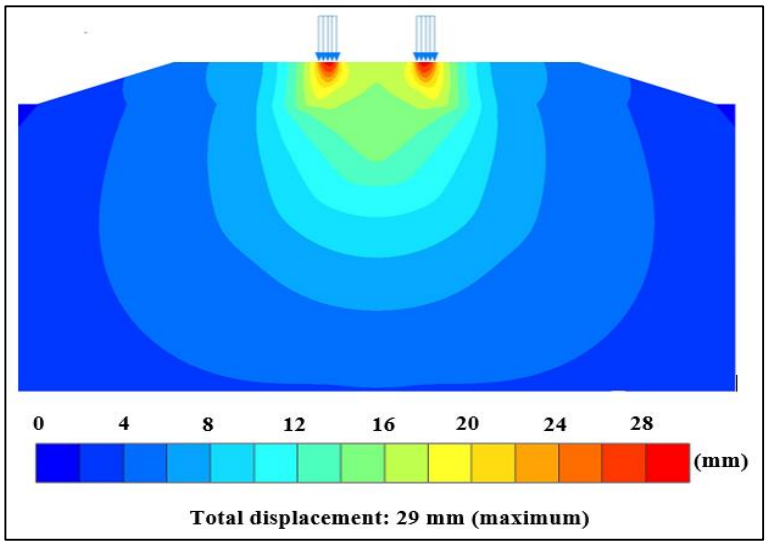

(b)

Figure 15. Modification in the total displacements for varying subgrade cohesion (a) $c_{s,min}$ = 2 kPa (b) $c_{sa,min}$ = 3.5 kPa

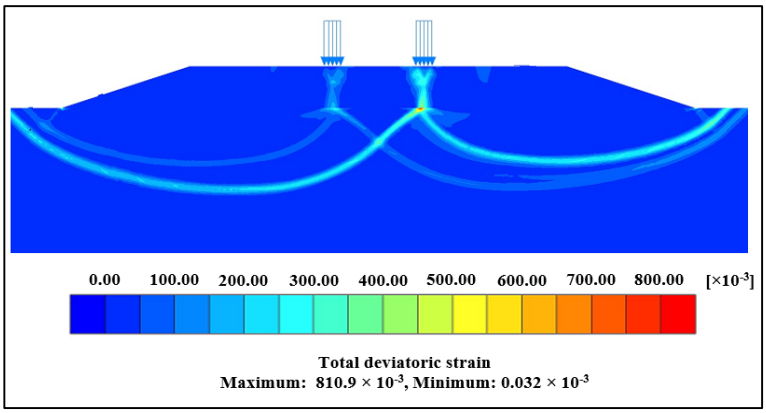

(a)

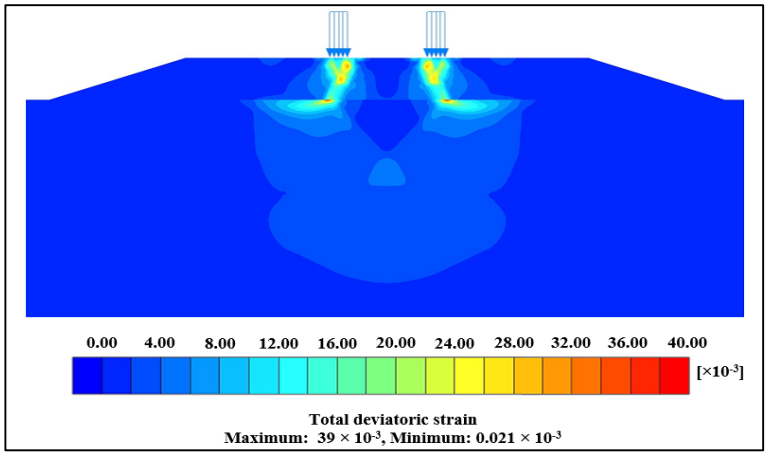

(b)

Figure 16. Modification in the total deviatoric strain for different subgrade cohesion magnitudes (a) $c_{s,min}$ = 2 kPa (b) $c_{sa,min}$ = 3.5 kPa

- **Step 15 / Final step**: Based on the analysis, assessments and inferences (as presented in the previous steps), the limiting cohesion of the aggregate and the subgrade ($c_{a,min}$ and $c_{sa,min}$: obtained from Step 8 and Step 13, respectively), along with their friction angles ($\varphi_{aggregate}$ and $\varphi_{subgrade}$), are considered to be the final strength parameters for this particular configuration of unpaved road system. This combination of strength parameters is capable in arresting the stresses from both operational aggregate loading and secondary stresses transmitted to the subgrade, thereby improving the overall sustainability and performance of the subgrade.

All the above-stated example simulations are undertaken with the aid of a 2.1 GHz Eight-Core Intel Xeon processor with 64-bit operating system. Depending on the vehicular axle load, the steps required to complete the design methodology might be different (as illustrated earlier in the two examples). Nevertheless, it is observed that any simulation is completed within 25-75 minutes, thereby exhibiting the computational efficacy of the proposed approach.

Conclusions and recommendations

This paper illustrates the necessity of adopting a coupled stress-deformation based approach in lieu of the conventionally adopted limit equilibrium-based approach for designing the unpaved roads. Finite element-based stress-deformation approach is administered to infuse a more realistic

703 design of the unreinforced unpaved road considering deformability of the individual components
704 and their response under operational loading conditions. Following are the important outcomes
705 and conclusions from the present study:

706 - A step-by-step design algorithm is provided to identify the aggregate and subgrade strength
707 parameters that would ensure the stability of unreinforced unpaved road subjected to
708 simultaneous aggregate and quasi-static vehicular loading.
709 - Following the conventional limit equilibrium based solutions considering non-deformable
710 components, analytical formulations are developed to determine the limiting cohesion
711 values of subgrade ($c_{s,min}$) and aggregate ($c_{a,min}$) layers that would satisfy the operational
712 stability of the individual components while being non-deformable. These assessments
713 should be used in the coupled stress-deformation approach in case the operational stability
714 of the of the individual components is not achieved.
715 - The importance of coupled stress-deformation based design approach is exclusively
716 highlighted for relatively weaker subgrades with low shear strength parameters and
717 recognizable deformability characteristics. It is revealed that even after using the aggregate
718 thickness (as estimated from existing analytical formulations), the subgrade can exhibit
719 failure under operational conditions due to the aggregate loading itself; thereby establishing
720 the necessity of improving the minimum cohesion of the subgrade to $c_{s,min}$.
721 - The FE analyses highlighted that the aggregate layer can be susceptible to operational
722 failure due to substantially high stress concentrations at the edges of the wheel leading to
723 the punching shear failure mechanism within the aggregate layer. Under such conditions,
724 sufficient strengthening of the aggregate layer is necessary by enhancing the limiting
725 cohesion in the aggregate layer to $c_{a,min}$.
726 - The coupled stress-deformation approach confirmed that a subgrade strengthened to meet
727 its operational stability under aggregate loading can still exhibit failure under higher axle
728 loads due to the generation of secondary stresses that are transferred from the aggregate
729 layer strengthened against its own individual operational stability. In such condition,
730 additional improvement in subgrade strength is required by heuristically enhancing the
731 minimum cohesion to $c_{sa,min}$.
732 - With the aid of the total and deviatoric strain concentration plots, the coupled stress-
733 deformation approach distinctly portrays various failure mechanism of unpaved road under

different parameter combinations. Upon incorporating the limiting cohesion components in the analyses, a recognizable change in the strain concentrations and slip lines are noticed that manifested arresting the extended failure mechanisms within confined regions of the domain.

This study presents a pioneering coupled stress-deformation based design algorithm in a finite element framework that addresses the design of unpaved roads considering a quasi-static vehicular loading. It is understood that the number of load repetitions play an instrumental role in the long-term performance of an unpaved road. Although this design algorithm does not directly include the same, it would take a little effort to include the influence of load repetitions on the assessments of accumulated residual deformations and strains, as the basic design principle remains the same for each passage of vehicular load. Furthermore, it may be noted that the sustained performance an unpaved road can be hampered by many conditions such as poorly controlled traffic and vehicular loading, climatic conditions and locations, and successive shear failures due to heavy rains. However, such scenarios need to be checked through response analysis of the designed section to ascertain its performance. Based on the outcomes arising out of these site-specific scenarios, the designed section might require necessary modifications and proper maintenance of the unpaved would be required to increase its longevity.

Declaration of Interest

The authors declare that there is no potential conflict of interest between the authors of this manuscript.

REFERENCES

Alzubaidi, H. and Magnusson, R. 2002. Deterioration and rating of gravel roads. *Road Materials and Pavement Design*, 3(3), 235-260.

Barber, V.C., Odom, E.C. and Patrick, R.W., 1978. *The deterioration and reliability of pavements*. Technical Report S-78-8, US Army Engineers Waterways Experiment Station, Vicksburg, Mississippi.

763 Barbieri, D.M., Hoff, I. and Mork, M.B.E. 2019. Innovative stabilization techniques for weak
764 crushed rocks used in road unbound layers: A laboratory investigation. *Transportation*
765 *Geotechnics*, 18, 132-141.

766 Barbieri, D.M., Hoff, I. and Mork, M.B.E. 2020. Organosilane and lignosulfonate as innovative
767 stabilization techniques for crushed rocks used in road unbound layers. *Transportation*
768 *Geotechnics*, 22, 1-14.

769 Boresi, A. and Palmer, J. 1995. Appraisal of models for unpaved roads. *In*: *Sixth International*
770 *Conference on Low-Volume Roads,* June 25-29 Minneapolis, Minnesota, 6, 147-156.

771 Burd, H. and Frydman, S. 1997. Bearing capacity of plane-strain footings on layered soils.
772 *Canadian Geotechnical Journal*, 34(2), 241-253.

773 CIA's The World Factbook, 2023. *Field Listings-Roadways*. Available from:
774 https://www.cia.gov/the-world-factbook/field/roadways [Accessed 6 June 2023].

775 Dey, A. and Meena, S. 2013. Geosynthetic reinforced unpaved road resting on *c-φ* subgrade"
776 *Indian Geotechnical Conference*, Roorkee, India, 1-10.

777 Diaz, J., Riveros, O. and Muñoz, M. 2020. Design of unpaved roads with DACE® software. *ARPN*
778 *Journal of Engineering and Applied Sciences*, 15(1), 1819-6608.

779 Douglas, R. and Valsangkar, A. 1992. Unpaved geosynthetic-built resource access roads: Stiffness
780 rather than rut depth as the key design criterion. *Geotextiles and Geomembranes*, 11(1), 45-59.

781 Edvardsson, K. 2009. Gravel roads and dust suppression. *Road Materials and Pavement Design*,
782 10(3), 439-469.

783 Freira, A.C., das Neves, J.M.C., Roque, A., Martins, I.M. and Antunes, M.L. 2021. Feasibility
784 study of milled and crushed reclaimed asphalt pavement for application in unbound granular
785 layers. *Road Materials and Pavement Design*, 22(7), 1500-1520.

786 Georgees, R.N. and Hassan, R. 2022. Performance-related properties of low-volume roads when
787 stabilised with a sustainable anionic polyacrylamide: particle and specimen-levels study. *Road*
788 *Materials and Pavement Design*, 23(3), 565-582.

789 Ghosh, P. and Kumar, S. 2011. Interference effect of two nearby strip surface footings on
790 cohesionless layered soil. *International Journal of Geotechnical Engineering,* 5(1):87-94.

791 Giroud, J. and Han, J. 2004. Design methods for geogrid-reinforced unpaved roads I-Development
792 of design method. *Journal of Geotechnical and Geoenvironmental Engineering*, 130(8), 775-786.

793 Giroud, J. and Noiray, L. 1981. Geotextile-reinforced unpaved road design. *Journal of*
794 *Geotechnical Engineering Division*, 107(9), 1233-1254.

795 Holtz, R and Sivakugan, N. 1987. Design charts for roads with geotextiles. *Geotextiles and*
796 *Geomembranes*, 5(3), 191-199.

797 Houlsby, G. and Burd, H. 1999. Understanding the behaviour of unpaved roads on soft clay.
798 *Twelfth European Conference on Soil Mechanics and Geotechnical Engineering (Proceedings)*,
799 Amsterdam, Netherlands, 1, 31-42.

800 Huber, S., Henzinger, C. and Heyer, D. 2020. Influence of water and frost on the performance of
801 natural and recycled materials used in unpaved roads and road shoulders. *Transportation*
802 *Geotechnics*, 22, 100305.

803 Ibagon, L. *et al.* 2023. Modelling of washboard effect on unpaved roads experimental evidence on
804 non-cohesive materials. *Transportation Geotechnics*, 41, 101015.

805 Indian Road Congress, 2008. *IRC: SP: 77, Manual for Design Construction and Maintenance of*
806 *Gravel Roads*, New Delhi.

807 Jones, D. and Paige-Green, P. 2015. Limitations of using conventional unpaved road specifications
808 for understanding unpaved road performance. *Transportation Research Record: Journal of the*
809 *Transportation Research Board*, 2474(1), 30-38.

810 Kuttah, D. 2016. The performance of a trial gravel road under accelerated pavement testing.
811 *Transportation Geotechnics*, 9, 161-174.

812 Lade, P.V. 2005. Overview of constitutive models for soils. *In: Geotechnical Special Publications*
813 *No.*, 128, pp 1-34.

814 le Vern, M., 2022. Effects of soil surface degradation and vehicle momentum on dust emissions
815 and visibility reduction from unpaved roads. *Transportation Geotechnics*, 37, 1-12.

816 Lopez-Uceda, A., Ayuso, J., Jimenez, J.R., Galvin, A.P. and Del Rey, I. 2020. Feasibility study of
817 roller compacted concrete with recycled aggregates asbase layer for light-traffic roads. *Road*
818 *Materials and Pavement Design*, 21(1), 276-278.

819 Magalhaes, A.J., Gomes, G.J.C. and Pires, P.J.M. 2022. Toward improved performance of
820 unpaved roads: laboratory tests and field investigation of a soil-byproduct base layer. *Road*
821 *Materials and Pavement Design*, 23(1), 184-198.

822 Meena, S., Choudhary, L. and Dey, A. 2013. Quasi-static analysis of geotextile-reinforced
823 unpaved road resting on c-φ subgrade. *Procedia – Social and Behavioral Sciences*, 104 (2), 235–
824 244.

825 Mendoza, A., *et al.* 2022. Mechanical behavior assessment of tire-reinforced recycled aggregates
826 for low traffic road construction. *Transportation Geotechnics*, 33, 1-8.

827 Miekos, E., Zielinski, M., Kolodziejczyk, K. and Jaksnder, M. 2019. Application of industrial and
828 biopolymers waste to stabilise the subsoil of road surfaces. *Road Materials and Pavement Design*,
829 20(2), 440-453.

830 Milligan, G., *et al*. 1989. A new approach to the design of unpaved roads – Part I. *Ground*
831 *Engineering*, 22(3), 25-29.

832 Milligan, G., *et al*. 1989. A new approach to the design of unpaved roads – Part II. *Ground*
833 *Engineering*, 22(3), 25-29.

834 Ministry of Road Transport and Highways, 2005. *Specification of maximum gross vehicle weight*
835 *and maximum safe axle weight*. Government of India, New Delhi.

836 MORTH, 2023. *Road Transport Year Book*, Government of India, Ministry of Road Transport and
837 Highways. Available from: https://morth.nic.in/sites/default/files/RTYB-2017-18-2018-19.pdf
838 [accessed 6 June 2023].

839 Paige-Green, P., Pinard, M. and Netterberg, F. 2015. A review of specifications for lateritic
840 materials for low volume roads. *Transportation Geotechnics*, 5, 86-98.

841 Pooni, J., Robert, D., Gisutozzi, F., Gunasekara, C. and Setunge, S. 2023. A review on soil
842 stabilisation of unsealed road pavements from an Australian perspective. *Road Materials and*
843 *Pavement Design*, 24(4), 1005-1049.

844 Poorahong, H., Jamsawang, P., Thanasisathit, N., Jongpradist, P. and Horpibulsuk, S. 2024.
845 Enhancing the bearing capacity of unpaved roads on soft clay subgrade using geogrid
846 reinforcement with a triaxial configuration. Construction and Building Materials 456(139321): 1-
847 12.

848 Ramdas, V.M., *et al.* 2021. Review of current and future bio-based stabilisation products
849 (enzymatic and polymeric) for road construction materials. *Transportation Geotechnics*, 27, 1-18.

850 Richards, R. 1978. Lightly trafficked roads in southern Africa. A review of practice and
851 recommendations for design NITRR Rep RP/8/78, Pretoria, South Africa.

852 Sarma, N.J. and Dey, A. 2024a. Improvement of long-term performance of unpaved road
853 constructed over marginalized subsoil using geotextile reinforcement. *International Journal of*
854 *Geosynthetics and Ground Engineering*, 10(Art. 39), 1-24. (DOI: https://doi.org/10.1007/s40891-
855 024-00550-6)

856 Sarma, N.J. and Dey, A. 2024b. Finite element based design and analysis of unpaved roads over
857 difficult subsoil: sustainable application of geotextile reinforcement to attain long-term
858 performance. *Indian Geotechnical Journal*, 54(3), 753-780. (DOI: https://doi.org/10.1007/s40098-
859 024-00866-0)

Shoop, S. *et al.* 2006. Seasonal deterioration of unsurfaced roads. *Journal of Geotechnical and Geoenvironmental Engineering*, 132(7), 852-860.

Terzaghi, K., 1943. *Bearing Capacity: Theoretical Soil Mechanics*. John Wiley and Son. New York.

Thogersen, F., Gregoire, C., Stryk, J., Hornych, P., Descantes, Y., Chazallon, C., Blasl, A., Broere, P., Bizjak, K.F., Hellman, F. and Arm, M. 2013. Recycling of road materials into new unbound road layers – main practice in selected European countries. *Road Materials and Pavement Design*, 21(1), 276-278.

Yaghoubi, E. *et al*. 2016. Stiffness properties of recycled concrete aggregate with polyethylene plastic granules in unbound pavement applications. *Journal of Materials in Civil Engineering*, 29(4), 04016271-1-7.

Figure Captions

Figure 1: A typical geometry of unreinforced unpaved road

Figure 2: Identification of optimal mesh size from a typical mesh convergence study

Figure 3: FE discretization and meshing of a typical unreinforced unpaved road geometry

Figure 4: Comparison of the load-settlement response between the experimental and FE results

Figure 5: Flowchart of proposed stress-deformation based design algorithm for unpaved roads

Figure 6: Comparison of bearing pressure vs settlement response between the experimental and FE results for the unreinforced unpaved road

Figure 7: (a) Development of secondary stresses in the subgrade due to combined aggregate and vehicular loading (b) Arresting of the developed secondary stresses within the aggregate layer by heuristically increasing the strength parameter of the subgrade equal to that achieved by geogrid-reinforced unpaved road section

Figure 8: FE model of unpaved road with subgrade subjected to aggregate loading

Figure 9: Strain-deformation response of subgrade subjected to aggregate loading considering basic parametric set as obtained from analytical modeling: (a) Total deviatoric strain shading (b) Incremental deviatoric strain shading (c) Plastic point distribution

Figure 10: Response of subgrade subjected to aggregate loading considering the improved strength parameter of subgrade: (a) Total deviatoric strain (b) Plastic point distribution

Figure 11: FE model of unreinforced unpaved road subjected to vehicular load

Figure 12: Response of the FE model of unreinforced unpaved road with basic strength parameters of aggregate layer and subjected to vehicular load (a) Total deviatoric strain (b) Total major principal strain and (c) Cartesian shear stress distributions

Figure 13: Response of subgrade subjected to vehicle loading considering the improved strength parameter of aggregate in terms of total deviatoric strain developed in the system

Figure 14: Response of the aggregate-subgrade system subjected to higher axle load after strength improvement of the aggregate layer: (a) Total deviatoric strain (b) Principal strain (c) Incremental deviatoric strain (d) Plastic points

Figure 15: Modification in the total displacements for varying subgrade cohesion (a) $c_{s,min}$ = 2 kPa (b) $c_{sa,min}$ = 3.5 kPa

Figure 16: Modification in the total deviatoric strain for different subgrade cohesion magnitudes (a) $c_{s,min}$ = 2 kPa (b) $c_{sa,min}$ = 3.5 kPa